A Class of Exact Solutions for Population Balances with Arbitrary Internal Coordinates

Tony Saad, Alex W. Abboud, Sean T. Smith, and Terry A. Ring
Dept. of Chemical Engineering, Institute for Clean and Secure Energy, University of Utah, Salt Lake City, UT 84112

DOI 10.1002/aic.14739
Published online in Wiley Online Library (wileyonlinelibrary.com)

We develop a novel transformation that maps the linear, nonhomogeneous, multidimensional population balance equation (PBE) into an advection equation that is readily solved using the method of characteristics. The PBEs targeted by this transformation exclude aggregation, breakage, and time dependent birth and death rates. In addition, internal coordinates are assumed to grow independently of each other. The ensuing general formulation is then used to recover closed-form analytical solutions for problems with monosurface and bulk-diffusion growth-rates as well as Gaussian-type nucleation. For completeness, we derive the multidimensional Green's functions for our approach. This is followed by a brief discussion on how the proposed framework may be used for code verification of moment methods such as the quadrature method of moments and the direct quadrature method of moments. Finally, a sample Mathematica code is provided to derive analytical solutions for the single-internal-coordinate case given user-specified growth, birth, and death rates. © 2015 American Institute of Chemical Engineers *AIChE J*, 00: 000–000, 2015
Keywords: mathematical modelling, particulate processes, population balance, precipitation, analytical methods, method of characteristics

Introduction

The analysis of reactive, dispersed-phase systems usually depends on an accurate representation of the behavior of particles, droplets or bubbles, their chemistry, and hydrodynamic interactions. This type of analysis is generally approached by solving some form of the population balance equation (PBE) coupled with momentum and species transport.

The solution to population balances is usually complicated due to the nature of the coupling between the particle distribution, its internal coordinates, and the mass balance requirements when precipitation and dissolution take place. While analytical methods provide detailed solutions to simple problems, numerical methods remain the key approach in resolving the dynamics of PBEs. The most notable numerical techniques to solve PBEs are the quadrature method of moments (QMOM) and the direct quadrature method of moments (DQMOM). These were pioneered by McGraw,[1,2] and Marchisio et al.[3–7] among others. Both QMOM and DQMOM aim at tracking the moments of the PBE, hence, much of the information contained in the particle distribution are smoothed by these methods. They remain, however, the most commonly used approaches.

Analytical solutions, conversely, provide an avenue for closed form, simple evaluations that help in identifying short- and long-term behavior of a particular model. They also serve as a benchmark for guiding experimental and numerical investigations.

There have been many efforts in the literature to derive analytical solutions for population balances under a variety of physical conditions. The most common approach employs a similarity transformation. Schumann,[8] as cited by Pulvermacher and Ruckenstein,[9] was probably the first to observe that the distribution of colloid particles may be represented by a single similarity variable. He made this observation while studying colloidal suspensions in fog. Later, Pulvermacher and Ruckenstein[9] made significant contributions to the use of similarity transforms by solving a two-dimensional coagulation equation. They identified the regions where similarity transforms exist and when a solution is admissible. Among other contributions, one may cite the work of Scott,[10] and Kapur and coworkers.[11,12]

Diemer and Olson[13–15] made further advances to the use of similarity transforms in a three-part study. Their work aimed at reconstructing the particle-size distribution from the moments by using a set of basis functions derived from the analytical solution for small-size particles in conjunction with information for large-size particles. Their analytical solution used a similarity transform congruent with previous results. Additional contributions by Diemer can be found in his two manuscripts published in 2006.[16,17]

In this study, we present a novel transformation that maps a special form of the multidimensional nonhomogeneous PBE into a homogeneous advection equation with the growth rates taking the role of the advecting velocities. The method requires that the birth and death terms be a function of the internal coordinates only. At the outset, this transformation

Correspondence concerning this article should be addressed to T. Saad at saadtony@gmail.com.

allows one to easily and systematically derive exact solutions for a population with an arbitrary number of internal coordinates using the method of characteristics. While it may be argued that all linear PBEs are amenable to analytical solutions, these usually lead to algebraic complications that require repeated derivation efforts if one desires to change the growth rates or source terms for instance. Our proposed transformation removes this complexity and casts the general solution for PBEs in a format that may be applied with little effort.

Compared to the similarity transform, the method of characteristics provides a time-accurate resolution of population dynamics while similarity transforms typically describe long-term (often asymptotic) behavior. Conversely, similarity transforms are more effective at handling nonlinear birth and death rates such as those occuring in aggregation and breakage.

The article is organized as follows. We first discuss our mathematical model for a single-internal-coordinate PBE. For convenience, a step-by-step approach to implementing the proposed transformation and deriving new solutions is developed. These steps are then used to derive analytical solutions for two hypothetical problems with monosurface and bulk-diffusion growth, respectively. We then generalize our transformation to PBEs with an arbitrary number of internal coordinates. This generalization entails the assumption that growth rates only depend on their corresponding internal coordinate. For completeness, we derive the multidimensional Green's functions and verify that they are congruent with the derived solution. This is followed by an overview of how these solutions may be used for code verification of numerical PBE solvers such as QMOM and DQMOM. Finally, a sample Mathematica code is provided for deriving analytical solutions for the single-internal-coordinate case given user-specified growth, birth, and death rates.

Mathematical Formulation

Consider a well-mixed reactor in which a population of particles with a single property of interest—or internal coordinate—such as size, composition, and so forth, is evolving in time. The assumption of a well-mixed reactor allows us to neglect hydrodynamic effects and is congruent with a well-mixed batch crystallizer. These are used consistently in modeling industrial processes and provide a valuable avenue for reduced-order models of complex systems. The initial condition in the reactor may correspond to a predefined seed distribution or a clean mixture with no particles. The particles are subsequently allowed to nucleate, grow, and dissolve.

To describe the temporal evolution of the particles in internal coordinate space, we employ the PBE for the number density function N. The number density function is defined as the number of particles per unit volume, per product of unit particle properties. At the outset, the PBE is given by[7,18,19]

$$\frac{\partial N(r,t)}{\partial t}+\frac{\partial g(r)N(r,t)}{\partial r}=h(r);\quad h(r)\equiv b(r)-d(r) \tag{1}$$

where $N(r,t)$ is the number density function, r is the internal coordinate, $g(r)$ is the growth rate defined as $g(r)=dr/dt$, and $b(r)$ and $d(r)$ are particle birth and death terms, respectively. Both $b(r)$ and $d(r)$ are assumed to be independent of $N(r,\ t)$ and time. As a consequence, this study excludes breakage and aggregation terms. For an analytical treatment of aggregation and breakage, the reader is referred to Vigil and Ziff[20] who derive steady-state solutions for a generalized coagulation-fragmentation equation. Finally, the initial condition is prescribed by $N_0(r)\equiv N(r,0)$.

Transformation

Being linear and first order, Eq. 1 may be solved using a variety of techniques such as the method of characteristics. However, in its current nonhomogeneous form, the solution of Eq. 1 leads to unnecessary algebraic complications that may prevent a complete solution in closed form.

Here, we introduce a novel transformation that maps Eq. 1 into a homogeneous partial differential equation that is easily amenable to a general solution. We define the modified number function $\eta(r,t)$ as

$$N(r,t)=\frac{1}{g(r)}\eta(r,t)+\frac{1}{g(r)}\int_0^r h(r')dr'. \tag{2}$$

Substitution of Eq. 2 into Eq. 1 yields the following homogeneous advection equation for $\eta(r,t)$

$$\frac{\partial \eta}{\partial t}+g(r)\frac{\partial \eta}{\partial r}=0, \tag{3}$$

where we used the following identities to arrive at Eq. 3

$$\frac{\partial N}{\partial t}=\frac{1}{g(r)}\frac{\partial \eta}{\partial t};\quad \frac{\partial g(r)N}{\partial r}=\frac{\partial \eta}{\partial r}+h(r). \tag{4}$$

The initial condition for η may be easily deduced from Eq. 2 by setting $t=0$. This operation gives

$$\eta_0(r)\equiv\eta(r,0)=g(r)N_0(r)-\int_0^r h(r')dr'. \tag{5}$$

Equation 3 is a first order, homogeneous, linear advection equation that can be readily solved using the method of characteristics.

Solution

The solution to Eq. 3 may be obtained by parametrizing η as follows. Let s denote the parametric variable for the characteristic curves and λ designates the initial point from which the characteristic curves evolve. This corresponds to the internal coordinate r such that $r(s=0)=\lambda$. Then, the total derivative of η along the characteristics may be written as

$$\frac{d\eta}{ds}=\frac{\partial \eta}{\partial t}\frac{dt}{ds}+\frac{\partial \eta}{\partial r}\frac{dr}{ds} \tag{6}$$

The right-hand-side of Eq. 6 has the same form as Eq. 3. In fact, these equations are made equal by setting

$$\frac{dt}{ds}=1\quad(a);\quad \frac{dr}{ds}=g(r)\quad(b);\quad \frac{d\eta}{ds}=0\quad(c). \tag{7}$$

Finally, we choose $t(s=0)=0$. At the outset, the initial conditions in the characteristic space correspond to a parametric curve $\mathcal{C}[t_0=0,\lambda,s=0,\eta_0(\lambda)]$.

The solution to Eq. 7 is straightforward. Starting with Eq. 7a, we recover $s=t$. Following through with Eq. 7b, it may be integrated as follows

$$\int_{r'(s=0)}^{r}\frac{1}{g(r')}dr'=\int_{\lambda}^{r}\frac{1}{g(r')}dr'=\int_0^s ds. \tag{8}$$

This equation will help us determine the relation between λ, r, and t. Also note the use of the identity $r(s=0)=\lambda$. To make further headway, we define

Table 1. A List of Common Growth Laws and Their Corresponding Characteristics

Growth Law	$g(r)$	$Q \equiv \int 1/g(r)dr$	Q^{-1}	λ
Linear	r	$\ln r$	e^r	re^{-t}
Monosurface	r^2	$-r^{-1}$	r^{-1}	$\frac{r}{1+rt}$
Bulk diffusion	r^{-1}	$\frac{1}{2}r^2$	$\pm\sqrt{2r}$	$\pm\sqrt{r^2-2t}$

$$Q(r) \equiv \int \frac{1}{g(r)} dr. \tag{9}$$

Then, Eq. 8 is conveniently written as

$$Q(r) - Q(\lambda) = s. \tag{10}$$

At the outset, the initial characteristic point may be obtained by solving

$$\lambda = Q^{-1}(Q(r) - t) \tag{11}$$

where Q^{-1} is the inverse function of $Q(r)$. Note that in Eq. 11, Q^{-1} is evaluated at $Q(r)-t$. An example is when $Q(r)=\ln r$. This leads to $Q^{-1}(r)=e^r$ and $\lambda=Q^{-1}(\ln r - t)=re^{-t}$. A summary of initial characteristic points λ as well as Q and Q^{-1} for some common growth laws is shown in Table 1. For additional growth-rate models Dirksen and Ring[21] provide a comprehensive overview of particle growth models for crystallization applications.

Lastly, the solution for η is found by integrating Eq. 7c. This yields

$$\eta(\lambda, s) = \eta_0(\lambda). \tag{12}$$

With $\eta(r,t)$ at hand, the number density function is obtained from Eq. 2

$$N(r,t) = \frac{g[\lambda(r,t)]}{g(r)} N_0[\lambda(r,t)] + \frac{1}{g(r)} \int_{\lambda(r,t)}^{r} h(r')dr'. \tag{13}$$

This equation stands as the general solution for Eq. 1. It may be viewed as the superposition of two responses; the first corresponding to the initial condition and the second corresponding to particle birth and death. These are easily identifiable in Eq. 13 and stand as the first and second terms on the right-hand-side of that equation, respectively.

Systematic implementation

Here, we present a step-by-step approach to obtain solutions for problems governed by Eq. 1. One may implement the following, preferably by their order of appearance:

1. Solve for $\lambda(r,t)$ using Eq. 11.
2. Substitute $\lambda(r,t)$ into the second term on the right-hand-side of Eq. 13.
3. Integrate the resulting expression.
4. Construct the general solution using Eq. 13 by making the necessary substitutions.

Applications

By way of illustration, we present two applications for using our proposed methodology. These sample problems, while academic in nature, have been used in practice to verify our QMOM implementation both as a standalone code and within a large scale, computational fluid dynamics, simulation tool.

Monosurface growth with Gaussian nucleation

For this example, we consider the monosurface growth of particles in a well-mixed reactor with an initial condition given by a lognormal distribution with $\mu = 0$ and $\sigma = 1/2$. This may be written as

$$N_0(r) = \ln \mathcal{N}(0, \frac{1}{2}) = \begin{cases} \sqrt{\frac{2}{\pi}} \frac{1}{r-1} e^{-2[\ln(r-1)]^2} & r > 1; \\ 0 & r \le 1. \end{cases} \tag{14}$$

The nucleation rate is given by a narrow Gaussian distribution centered at $r = 1$ to mimic the behavior of constant particle birth at a given critical radius. This is given by

$$b(r) = \frac{12}{\sqrt{\pi}} e^{-144(r-1)^2}, \quad \forall\, t > 0. \tag{15}$$

This model may be used, for example, in analyzing the precipitation of solids from a liquid solution. In practice, the critical radius may change with supersaturation, nonetheless, the current assumption of a fixed critical radius is a viable leading order approximation.

Using the procedure outlined in the previous section one arrives at the following solution for the number density function

$$N(r,t) = \left\{ \begin{array}{ll} \sqrt{\frac{2}{\pi}} \frac{1}{(r-rt-1)(rt+1)} e^{-2[\ln(\lambda-1)]^2} & \lambda > 1 \\ 0 & \text{otherwise} \end{array} \right\} + \frac{1}{r^2}\text{Erf}[12(r-1)] - \frac{1}{r^2}\text{Erf}[12(\lambda-1)] \tag{16}$$

where $\lambda = r/(rt+1)$.

One can also deduce the steady-state behavior of the particles by taking the limit of Eq. 16 as $t \to \infty$. This yields

$$N(r) = \frac{1}{r^2}\text{Erf}[12(r-1)] + \frac{1}{r^2}. \tag{17}$$

The solution given in Eq. 16 is shown in Figure 1 at different dimensionless times. Starting with $t = 0$ in Figure 1a, the initial condition clearly shows the log-normal distribution. The effect of the narrow Gaussian nucleation is visible in Figures 1b, c, and d with a spike in the number of particles at $r = 1$, our chosen critical radius. Finally, the steady-state solution is shown in Figure 1e where the nucleation rate clearly dominates while the effect of the initial condition is "washed-out" as the initial particles had ample time to grow and advect along the particle-size dimension.

Bulk-diffusion growth with Gaussian nucleation

For this problem, we reconsider the conditions given in the previous example with the exception of using bulk-diffusion growth instead of monosurface growth. In this case, the solution is easily obtained as

$$N(r,t) = \left\{ \begin{array}{ll} \sqrt{\frac{2}{\pi}} \frac{r}{r^2-\lambda-2t} e^{-2[\ln(\lambda-1)]^2} & \lambda > 1 \\ 0 & \text{otherwise} \end{array} \right\} + r\text{Erf}[12(r-1)] - r\text{Erf}[12(\lambda-1)] \tag{18}$$

where $\lambda = \sqrt{r^2-2t}$.

Note, however, that due to the nature of the bulk-diffusion growth coupled with a birth rate at a fixed critical radius, the

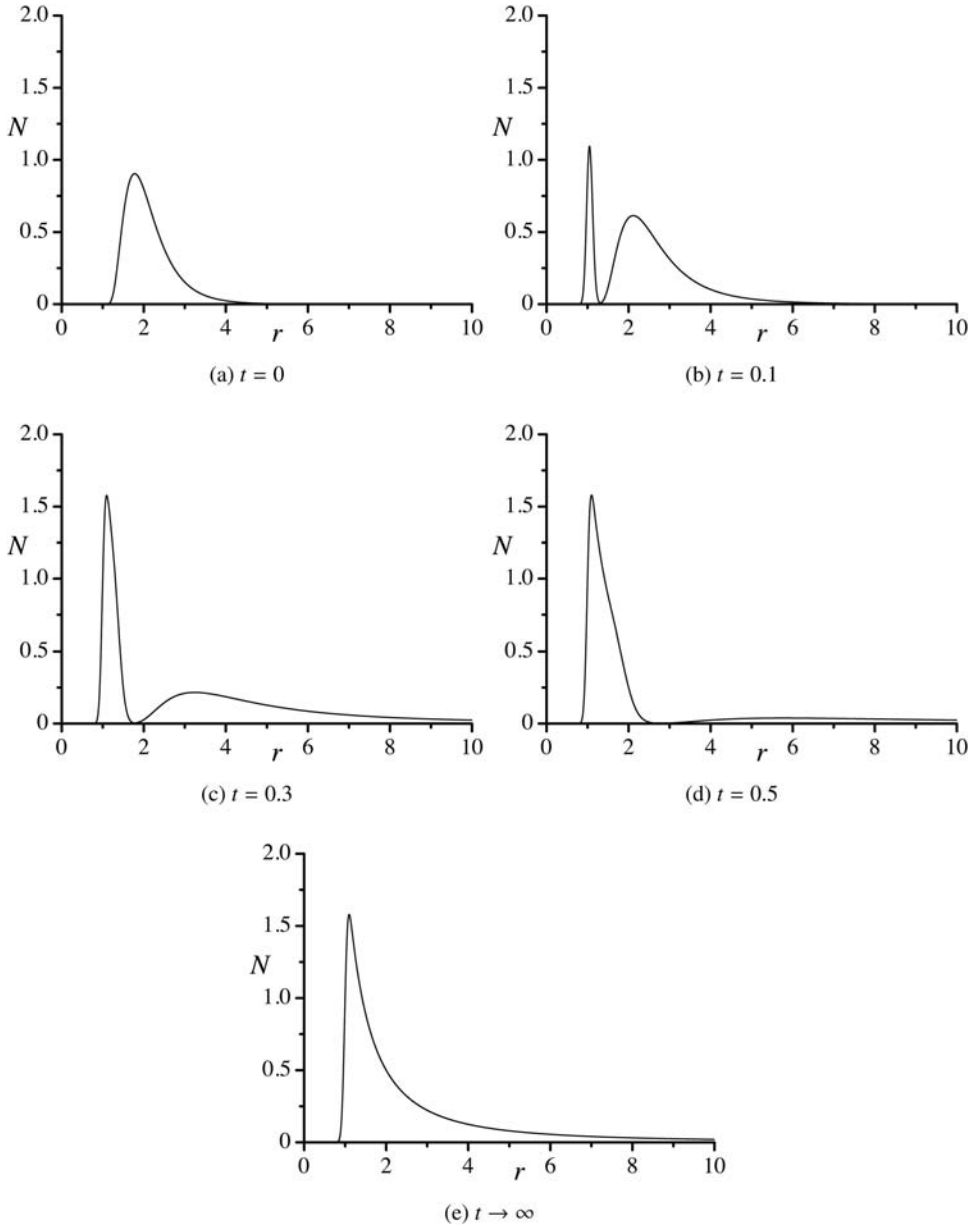

Figure 1. Evolution of particles with monosurface growth and Gaussian nucleation taken at various dimensionless times, t= (a) 0, (b) 0.1, (c) 0.3, (d) 0.5, and (e) steady state.

solution is valid so long as $r^2 \geq 2t$. This will cause unrealistic behavior when $r < \sqrt{2t}$. In practice, the critical radius is a function of time and additional system complexity resolves this problem by virtue of additional physics incorporated into the model. Nonetheless, it is interesting to look at the current case within the allowable range. The solution is shown in Figure 2 with samples taken at $t = 0.25$ and $t = 0.5$, spanning the time range allowed by the constraint $r^2 \geq 2t$.

Generalization

One may generalize the transformation given in Eq. 2 to multivariate PBEs provided that the growth rates are assumed to be a function of their corresponding internal coordinate only. In this case, the multivariate PBE for the number density function may be written as

$$\frac{\partial N(\mathbf{r},t)}{\partial t}+\sum_{i=1}^{m}\frac{\partial g_i(r_i)N(\mathbf{r},t)}{\partial r_i}=h(\mathbf{r}); \quad h(\mathbf{r}) \equiv b(\mathbf{r})-d(\mathbf{r}) \tag{19}$$

where, as before, $N(\mathbf{r},t)$ is the number density function, r_i is the ith internal coordinate, $\mathbf{r} \equiv (r_1, r_2, \cdots, r_m)$ is the internal coordinate vector, m is the number of internal coordinates, $g_i(r_i)$ is the growth rate of the ith internal coordinate, and $h(\mathbf{r}) \equiv b(\mathbf{r})-d(\mathbf{r})$ is a particle birth/death term that is independent of $N(\mathbf{r},t)$. In this case, the initial condition is also prescribed by $N_0(\mathbf{r}) \equiv N(\mathbf{r},0)$.

Multidimensional transformation

The one-dimensional transformation is now generalized by redefining the modified number density function $\eta(\mathbf{r},t)$ as

$$\begin{aligned} N(\mathbf{r},t) &\equiv \frac{1}{G(\mathbf{r})}\eta(\mathbf{r},t)+\frac{1}{G(\mathbf{r})}\int_0^s G[\mathbf{r}(s')]h[\mathbf{r}(s')]ds'; \\ G(\mathbf{r}) &\equiv \prod_{i=1}^{m} g_i(r_i), \end{aligned} \tag{20}$$

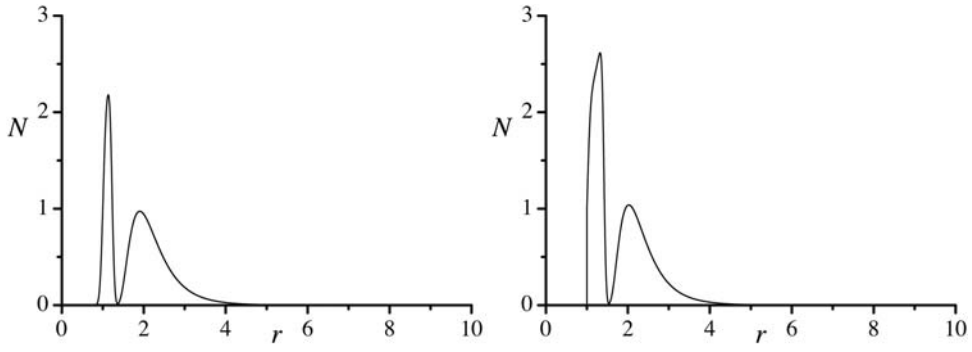

Figure 2. Evolution of particles with bulk-diffusion growth and Gaussian nucleation taken at t= (a) 0.25 and (b) 0.5.

where s denotes the parametric variable for the characteristic curves and $\lambda \equiv (\lambda_1, \lambda_2, \cdots, \lambda_m)$ designates the set of initial points from which the characteristic curves evolve.

The second term on the right-hand-side of Eq. 20 is a particular solution of Eq. 19. This term must be integrated in characteristic space first. The result is then mapped back into the internal coordinate space by substituting $\lambda_i \equiv \lambda(r_i, t)$. To show that this term is a particular solution of Eq. 19, we set

$$N(\mathbf{r}, t) \equiv \frac{1}{G(\mathbf{r})} B(\mathbf{r}, t) \tag{21}$$

then, on substitution into Eq. 19, we recover the following advection equation

$$\frac{\partial B(\mathbf{r}, t)}{\partial t} + \sum_{i=1}^{m} g_i(r_i) \frac{\partial B(\mathbf{r}, t)}{\partial r_i} = G(\mathbf{r}) h(\mathbf{r}, t); \quad B(\mathbf{r}, 0) = 0. \tag{22}$$

Using the method of characterisitics, the solution of Eq. 22 is

$$B(\mathbf{r}, t) = \int_0^s G[\mathbf{r}(s'), t] h[\mathbf{r}(s')] ds'. \tag{23}$$

Given that Eq. 22 shares the same characteristics as Eq. 19, one concludes that the particular solution of Eq. 22 is also a particular solution of Eq. 19.

Moving on, we substitute Eq. 20 into the general PBE and recover a homogeneous version of Eq. 19 with the modified number density η as the dependent variable. The resulting equation may be written as

$$\frac{\partial \eta(\mathbf{r}, t)}{\partial t} + \sum_{i=1}^{m} g_i(r_i) \frac{\partial \eta(\mathbf{r}, t)}{\partial r_i} = 0. \tag{24}$$

The initial condition for η is inferred from Eq. 20 by setting $t = 0$. This gives

$$\eta_0(\mathbf{r}) \equiv \eta(\mathbf{r}, 0) = G(\mathbf{r}) N_0(\mathbf{r}). \tag{25}$$

As before, Eq. 24 can now be readily solved using the method of characteristics.

Solution

Let s denote the parametric variable for the characteristic curves and $\lambda \equiv (\lambda_1, \lambda_2, \cdots, \lambda_m)$ designate the set of initial points from which the characteristic curves evolve. These correspond to the m internal coordinates $(r_1, r_2, \cdots, r_m)$ such that $r_i(s=0) = \lambda_i$. Finally, we set $t(s=0) = 0$. Starting on a curve $\mathcal{C}[t_0, \lambda, s=0, \eta_0(\lambda)]$, the characteristic equations are given by

$$\frac{dt}{ds} = 1 \quad \text{(a)}; \quad \frac{dr_i}{ds} = g_i(r_i) \quad \text{(b)}; \quad \frac{d\eta}{ds} = 0 \quad \text{(c)}. \tag{26}$$

These equations are now solved as follows. Starting with Eq. 26a, we have $s = t$. Integration of Eq. 26b yields

$$\int_{r_i(\lambda, s=0)}^{r_i} \frac{1}{g_i(r')} dr' = \int_{\lambda_i}^{r_i} \frac{1}{g_i(r')} dr' = \int_0^s ds. \tag{27}$$

This equation dictates the relation between λ_i, r_i, and t. In a manner to similar to Eq. 9, one defines

$$Q_i(r_i) \equiv \int \frac{1}{g_i(r_i)} dr_i. \tag{28}$$

Then, Eq. 27 is simplified to

$$Q_i(r_i) - Q_i(\lambda_i) = s. \tag{29}$$

At the outset, the general solution for the characteristic point associated with the ith internal coordinate is obtained by solving

$$\lambda_i = Q_i^{-1}(Q_i(r_i) - t) \tag{30}$$

where Q_i^{-1} is the inverse function of $Q_i(r_i)$.

An interesting relation for the characteristic points emerges from Eq. 30. Let $\xi \equiv Q_i(r_i) - t$, then, one can show that

$$\frac{\partial \lambda_i}{\partial t} = -\frac{dQ_i^{-1}}{d\xi} \quad \text{(a)}; \quad \frac{\partial \lambda_i}{\partial r_i} = \frac{1}{g_i(r_i)} \frac{dQ_i^{-1}}{d\xi} \quad \text{(b)} \tag{31}$$

from which one can easily deduce the following transport equation for λ_i

$$\frac{\partial \lambda_i}{\partial t} + g_i(r_i) \frac{\partial \lambda_i}{\partial r_i} = 0. \tag{32}$$

Lastly, the solution for η is found by integrating Eq. 26c

$$\eta(\lambda, s) = \eta_0(\lambda). \tag{33}$$

With $\eta(\mathbf{r}, t)$ at hand, the general solution for the number density function is obtained from Eq. 20

$$N(\mathbf{r}, t) = \frac{G(\lambda)}{G(\mathbf{r})} N_0(\lambda) + \frac{1}{G(\mathbf{r})} \int_0^s G(\lambda, s') h(\lambda, s') ds'. \tag{34}$$

Systematic implementation

Here, we present a step-by-step approach to obtain the solution for a particular problem governed by Eq. 19. One

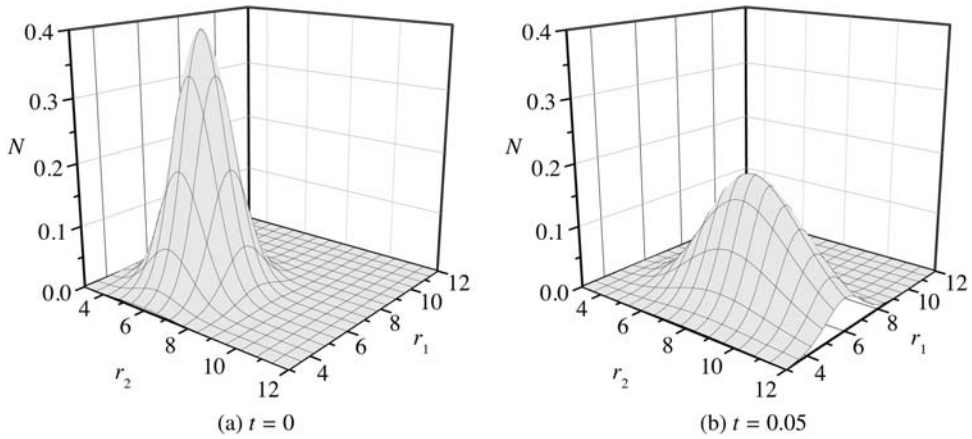

Figure 3. Evolution of particles with two internal coordinates growing according to monosurface and bulk-diffusion laws, respectively.

Figures show distribution at t= (a) 0 and (b) 0.05.

may implement the following, preferably by their order of appearance,

1. Solve for λ using Eq. 30.
2. With knowledge of $\lambda \equiv \lambda(\mathbf{r}, s)$, solve for $\mathbf{r} \equiv \mathbf{r}(\lambda, s)$.
3. Substitute $\mathbf{r} \equiv \mathbf{r}(\lambda, s)$ into the particular solution – the second term on the right-hand-side of Eq. 34.
4. Integrate the resulting expression in characteristic space.
5. Substitute $s = t$ and $\lambda_i \equiv \lambda_i(r_i, t)$.
6. Construct the general solution from Eq. 34 by making the necessary substitutions.

Example: Multivariate Monosurface and Bulk-Diffusion Growth

For this example, we consider the evolution of particles with two internal coordinates designated by r_1 and r_2. We use monosurface growth for r_1 and bulk-diffusion growth for r_2 to allow for interesting dynamics in the solution. The birth rate is assumed to be zero. It is possible for different growth mechanisms to operate separately on different internal coordinates. Such a case occurs for example in $CaCO_3$ precipitation where four known polymorphs, namely, amorphous calcium carbonate (ACC), Vaterite, Aragonite, and Calcite grow according to different mechanisms as the supersaturation ratio changes.[22] The initial condition is given by a symmetric two-dimensional normal distribution centered at $(r_1, r_2) = (6, 6)$ to avoid nonzero values in the negative domain

$$N_0(\mathbf{r}) = \frac{1}{\sqrt{2\pi}} \exp\left[-\frac{1}{2}(r_1-6)^2 - \frac{1}{2}(r_2-6)^2\right]. \quad (35)$$

We are now ready to apply the steps outlined in the previous section. However, in the absence of a source term, only the first step is needed. One is required to evaluate the characteristic points and perform the necessary substitutions into the initial condition. At the outset, the solution is given by

$$N(r_1, r_2, t) = \frac{1}{\sqrt{2\pi}} \frac{r_2}{(1+r_1 t)^2 \sqrt{r_2^2 - 2t}} e^{-\frac{1}{2}\left(\frac{r_1}{1+r_1 t}-6\right)^2 - \frac{1}{2}\left(\sqrt{r_2^2-2t}-6\right)^2}. \quad (36)$$

The time evolution of the distribution for this two-dimensional case is shown in Figure 3 at $t = 0$ and $t = 0.05$ in dimensionless time. The effect of the different growth rates is clearly visible in Figure 3b where the monosurface growth term dominates in the evolution of the initial distribution. This type of growth may be used, for example, to model anisotropic crystal or aerosol growth where the internal coordinates may be chosen to correspond to different lattice directions.

Green's Functions

Green's functions provide a very useful tool to obtain general analytical solutions for nonhomogeneous, linear partial differential equations (PDEs). The Green's function for a PDE represents its solution subject to arbitrarily located point sources and initial conditions. Once the Green's function is known, the solution to the PDE with analytic initial or forcing functions is easily obtained via a convolution with the Green's function.

For completeness, we briefly present the Green's functions for the PBE presented in Eq. 19. This is achieved by splitting the problem into two; the first corresponds to the homogeneous PBE with a nonzero, point-type initial condition while the second represents the contribution of particle birth or death with a zero initial condition. These may be written in mathematical form as

$$\frac{\partial E_h(\mathbf{r}, t; \mathbf{r}^*)}{\partial t} + \sum_{i=1}^{m} \frac{\partial g_i(r_i) E_h(\mathbf{r}, t; \mathbf{r}^*)}{\partial r_i} = 0; \quad E_h(\mathbf{r}, 0; \mathbf{r}^*) = \delta(\mathbf{r} - \mathbf{r}^*), \quad (37)$$

$$\frac{\partial E_s(\mathbf{r}, t; \mathbf{r}^*)}{\partial t} + \sum_{i=1}^{m} \frac{\partial g_i(r_i) E_s(\mathbf{r}, t; \mathbf{r}^*)}{\partial r_i} = \delta(\mathbf{r} - \mathbf{r}^*); \quad E_s(\mathbf{r}, 0; \mathbf{r}^*) = 0. \quad (38)$$

Here, E_h and E_s correspond to the Green's functions for the homogeneous and nonhomogeneous problems, respectively. Note that, $\mathbf{r}^* \equiv (r_1^*, r_2^*, \cdots)$ is an arbitrarily chosen parameter that designates the location of the point source, and $\delta(\mathbf{r} - \mathbf{r}^*) \equiv \delta(r_1 - r_1^*)\delta(r_2 - r_2^*) \cdots \delta(r_m - r_m^*)$ is the multi-dimensional Dirac delta function centered at $\mathbf{r}^*$ such that

$$\int_{-\infty}^{\infty} f(r_1, r_2, \cdots, r_m)\delta(\mathbf{r} - \mathbf{r}^*) dr = f(r_1^*, r_2^*, \cdots, r_m^*). \quad (39)$$

The solutions to Eqs. 37 and 38 are easily obtained by using Eq. 20. They are given by

$$E_h(\mathbf{r},t;\mathbf{r}^*)=\frac{G(\lambda)}{G(\mathbf{r})}\delta(\lambda-\mathbf{r}^*), \tag{40}$$

$$E_s(\mathbf{r},t;\mathbf{r}^*)=\frac{1}{G(\mathbf{r})}\int_0^s G[\mathbf{r}(s)]\delta[\mathbf{r}(s)-\mathbf{r}^*]ds=\begin{cases}\dfrac{G[\mathbf{r}(s)]}{G(\mathbf{r})} & 0\le\mathbf{r}^*\le s;\\ 0 & \text{otherwise.}\end{cases} \tag{41}$$

The general solution to the number density function N is then constructed via the following convolutions

$$N(\mathbf{r},t)=\int_{-\infty}^{\infty}N(\mathbf{r},0)E_h(\mathbf{r},t;\mathbf{r}^*)d\mathbf{r}^*+\int_{-\infty}^{\infty}h(\mathbf{r})E_s(\mathbf{r},t;\mathbf{r}^*)d\mathbf{r}^*. \tag{42}$$

Upon substitution of E_h and E_s, we recover the following solution for N

$$N(\mathbf{r},t)=\frac{G(\lambda)}{G(\mathbf{r})}N_0(\lambda)+\frac{1}{G(\mathbf{r})}\int_0^s G(\lambda,s')h(\lambda,s')ds' \tag{43}$$

which is identical to the general solution shown in Eq. 34.

Code Verification

The general solutions shown in Eqs. 13 and 34 may be used for verification of quadrature and DQMOM codes as well as other numerical techniques for the solution of PBEs. Code verification is an important aspect of modern code development and it is essential to have a robust and properly benchmarked population balance module as part of any larger-scale code. The process of code verification in this case may be accomplished using the following approach:

1. Obtain an analytical solution for a hypothetical problem such as the ones illustrated in this article.

2. If possible, obtain analytical solutions for the moments. While this may not be realizable in general, the moments may be calculated using numerical integration.

3. Compare results obtained from QMOM or DQMOM numerical solutions to those obtained from the analytical solution.

Here, we assumed that the order of accuracy in the discretization process has been properly verified and one is concerned with verification of the population balance physics. For a detailed overview of code verification, the reader is referred to the book by Oberkampf and Roy.[23]

Conclusions

We developed a novel transformation that maps the nonhomogeneous, multidimensional PBE into a simple advection equation. This transformation targets those population balance models in which the growth rates depend on their corresponding internal coordinate and exclude aggregation, breakage, and time-dependent birth and death rates. The presented approach allows for a systematic and straightforward solution methodology for PBEs. While the method of characteristics may be used to solve the PBE models considered in this study, the algebraic complexity introduced by solving the original equations becomes burdensome. Our suggested framework allows for significant reduction in the algebraic complexity associated with integrating the characteristic equations, to the extent that new solutions may be obtained with straightforward substitutions. This solution process was summarized via a sequence of easy-to-implement steps and was used to derive analytical solutions for three hypothetical problems. In all cases, the solution was presented in closed form and graphed at several times to illustrate its behavior. For added verification, we derived the multidimensional Green's functions for our targeted PBEs and showed that these match the solution obtained via direct integration of the original problem. Finally, we gave an overview of how the current solution framework may be used as an avenue for code verification of numerical PBE solvers. While analytical solutions are usually limited to simple problems, it is gratifying to add a new tool to our arsenal that may be used for academic purposes as well as for analyzing limiting system behavior in practical applications. Our transformation provides a utility to learn and apply population balances with minimal effort so that its use encourages focusing on population physics rather than the mathemtical complexity associated with their solution.

Sample Mathematica Code

The following Mathematica code may be used to obtain analytical solutions for the one-dimensional PBE with user-specified growth, birth, and death rates.

```
(* USEFUL FUNCTIONS *)
gaussian[ a_,  x_] = 2/(a  Sqrt[ Pi] )  Exp[ -x^2/
a^2] ;
(* USER INPUT *)
N0[ x_] :=   PDF[ LogNormalDistribution[ 0,   1/
2] , x - 1] ;
Growth[ x_] := x^2;
Birth[ x_] := gaussian[ 1/12, x - 1] ;
Death[ x_] := 0.01*gaussian[ 1/12, x - 2] ;

(* ———————————————————————————————————————*)
(* MAIN CODE *)

(* COMPUTE CHARACTERISTIC *)
Q[ x_] := Integrate[ 1/Growth[ x] , x] ;
l[ x_, t_] = l1 /. Solve[ Q[ x]  - t - Q[ l1]  == 0,
l1][[ 1]][[ 1]] ;

(*  COMPUTE  INDEFINITE  INTEGRALS  OF  GROWTH,
BIRTH, AND DEATH *)
IntGrowth[ x_] = Integrate[ Growth[ x] , x] ;
IntBirth[ x_] = Integrate[ Birth[ x] , x] ;
IntDeath[ x_] = Integrate[ Death[ x] , x] ;

(* COMPUTE RESPONSE TO BIRTH/DEATH *)
RHS[ x_, t_] = 1/Growth[ x]  (IntBirth[ x]
- IntBirth[ l[ x, t]] - IntDeath[ x] +
  IntDeath[ l[ x, t]] );

(* COMPUTE TOTAL SOLUTION *)
ND[ r_,   t_] :=   Growth[ l[ r,   t]] /Growth[ r]
N0[ l[ r, t]] + RHS[ r,t] ;

(* END MAIN CODE *)
(* ———————————————————————————————————————*)

(* EXAMPLE ANIMATION PLOT *)
Animate[ Plot[ { ND[ x, t] } , { x, 0, 10} ,
  PlotRange -> { Full, { 0, nMax} } , Filling ->
  Axis,
  PlotPoints -> 100] , { t, 0, 1} , { nMax, 1.75,
  3, 0.0001} ,
AnimationRunning -> False]
```

Acknowledgments

This research was sponsored by the National Nuclear Security Administration under the Advanced Simulation and Computing program through DOE Research Grant # DE-NA0000740. The authors would like to thank Ben Schroeder for reviewing this manuscript.

Literature Cited

1. McGraw R. Description of aerosol dynamics by the quadrature method of moments. *Aerosol Sci Technol*. 1997;27:255–265.
2. McGraw R, Nemesure S, Schwartz SE. Properties and evolution of aerosols with size distributions having identical moments. *J Aerosol Sci*. 1998;29:761–772.
3. Marchisio DL, Pikturna JT, Fox RO, Vigil RD, Barresi AA. Quadrature method of moments for population-balance equations. *AIChE J*. 2003a;49:1266–1276.
4. Marchisio DL, Vigil RD, Fox RO. Quadrature method of moments for aggregation-breakage processes. *J Colloid Interface Sci*. 2003b; 258:322–334.
5. Marchisio DL, Fox RO. Solution of population balance equations using the direct quadrature method of moments. *J Aerosol Sci*. 2005; 36:43–73.
6. Marchisio DL, Soos M, Sefcik J, Morbidelli M, Barresi AA, Baldi G. Effect of fluid dynamics on particle size distribution in particulate processes. *Chem Eng Technol*. 2006;29:191–199.
7. Marchisio DL, Fox RO, editors. *Multiphase Reacting Flows: Modelling and Simulation. CISM Courses and Lectures*. Springer Verlag, 2007.
8. Schumann T. Theoretical aspects of the size distribution of fog particles. *Q J Royal Meteorol Soc* 1940;66:195–208.
9. Pulvermacher B, Ruckenstein E. Similarity solutions of population balances. *J Colloid Interface Sci*. 1974;46:428–436.
10. Scott WT. Analytic studies of cloud droplet coalescence I. *J Atmos Sci*. 1968;25:54–65.
11. Kapur PC, Fuerstenau DW. Coalescence model for granulation. *Indus Eng Chem Process Des Dev* 1969;8:56–62.
12. Kapur P. Self-preserving size spectra of comminuted particles. *Chem Eng Sci*. 1972;27:425–431.
13. Diemer RB, Olson JH. A moment methodology for coagulation and breakage problems: part 2—moment models and distribution reconstruction. *Chem Eng Sci*. 2002a;57:2211–2228.
14. Diemer RB, Olson JH. A moment methodology for coagulation and breakage problems: part 1—analytical solution of the steady-state population balances. *Chem Eng Sci*. 2002b;57:2193–2209.
15. Diemer RB, Olson JH. A moment methodology for coagulation and breakage problems: part 3—generalized daughter distribution functions. *Chem Eng Sci*. 2002c;57:4187–4198.
16. Diemer RB, Olson JH. Bivariate moment methods for simultaneous coagulation, coalescence and breakup. *J Aerosol Sci*. 2006;37:363–385.
17. Diemer RB, Olson JH. Criterion for employing bivariate formulations in collision-coalescence problems. *J Aerosol Sci*. 2006;37: 1883–1887.
18. Ramkrishna D. *Population Balances*. San Diego, CA: Academic Press, 2000.
19. Randolph AD, Larson MA. *Theory of Particulate Processes*. New York: Academic Press, 1971.
20. Vigil R, Ziff RM. On the stability of coagulation and fragmentation population balances. *J Colloid Interface Sci*. 1989;133:257–264.
21. Dirksen JA, Ring TA. Fundamentals of crystallization: kinetic effects on particle size distributions and morphology. *Chem Eng Sci*. 1991; 46:2389–2427.
22. Schroeder B, Harris D, Smith S, Lignell D. Theoretical framework for multiple-polymorph particle precipitation in highly supersaturated systems. *Cryst Growth Des*. 2014;14(4):1756–1770.
23. Oberkampf WL, Roy CJ. *Verification and Validation in Scientific Computing*. Cambridge University Press, 2010.

Manuscript received Oct. 16, 2014, and revision received Dec. 15, 2014.